



# Enhanced mixing across the gyre boundary at the Gulf Stream front

Jacob O. Wenegrat<sup>a,1</sup>, Leif N. Thomas<sup>b</sup>, Miles A. Sundermeyer<sup>c</sup>, John R. Taylor<sup>d</sup>, Eric A. D'Asaro<sup>e</sup>, Jody M. Klymak<sup>f</sup>, R. Kipp Shearman<sup>g</sup>, and Craig M. Lee<sup>e</sup>

<sup>a</sup>Department of Atmospheric and Oceanic Science, University of Maryland, College Park, MD 20742; <sup>b</sup>Earth System Science, Stanford University, Stanford, CA 94305; <sup>c</sup>Department of Estuarine and Ocean Sciences, University of Massachusetts Dartmouth, North Dartmouth, MA 02747; <sup>d</sup>Department of Applied Mathematics and Theoretical Physics, University of Cambridge, Cambridge CB2 1TN, United Kingdom; <sup>e</sup>Applied Physics Laboratory, University of Washington, Seattle, WA 98105; <sup>f</sup>School of Earth and Ocean Sciences, University of Victoria, Victoria, BC V8P 5C2, Canada; and <sup>g</sup>College of Earth, Ocean, and Atmospheric Sciences, Oregon State University, Corvallis, OR 97331

Edited by Carl Wunsch, Harvard University, Cambridge, MA, and approved June 11, 2020 (received for review March 24, 2020)

**The Gulf Stream front separates the North Atlantic subtropical and subpolar ocean gyres, water masses with distinct physical and biogeochemical properties.** Exchange across the front is believed to be necessary to balance the freshwater budget of the subtropical gyre and to support the biological productivity of the region; however, the physical mechanisms responsible have been the subject of long-standing debate. Here, the evolution of a passive dye released within the north wall of the Gulf Stream provides direct observational evidence of enhanced mixing across the Gulf Stream front. Numerical simulations indicate that the observed rapid cross-frontal mixing occurs via shear dispersion, generated by frontal instabilities and episodic vertical mixing. This provides unique direct evidence for the role of submesoscale fronts in generating lateral mixing, a mechanism which has been hypothesized to be of general importance for setting the horizontal structure of the ocean mixed layer. Along the Gulf Stream front in the North Atlantic, these observations further suggest that shear dispersion at sharp fronts may provide a source of freshwater flux large enough to explain much of the freshwater deficit in the subtropical-mode water budget and a flux of nutrients comparable to other mechanisms believed to control primary productivity in the subtropical gyre.

oceanography | ocean mixing | Gulf Stream | submesoscale instabilities

The boundary between the subtropical and subpolar gyres of the North Atlantic is marked by the Gulf Stream front, where lateral gradients in temperature, salinity, density, and nutrients are extremely large (Fig. 1). It is thought that lateral fluxes of nutrients across the front play a critical role in closing nutrient budgets in the subtropical gyre and in providing the phosphate needed to maintain nitrogen fixation there (1–5). Analogously, the flux of cool, low-salinity water across the front has been implicated in the heat and salinity budgets of Eighteen Degree Water—a weakly stratified, voluminous water mass in the subtropical gyre thought to contribute to decadal climate variability (6). However, the physical processes that are responsible for mixing these tracers across the front are not well understood. Fronts by definition are characterized by enhanced tracer gradients—which would tend to be eroded in the presence of significant cross-frontal mixing. Strain associated with large-scale confluent flow provides a mechanism for generating and maintaining the strong gradients; however, these flows are often approximately two-dimensional in the horizontal, suggesting that the fronts will act as dynamical barriers to cross-frontal transport and mixing (7). On the other hand, their strong currents provide a source of energy for turbulent motions such as eddies that can blend the disparate water masses across the front. The debate as to whether the Gulf Stream front in particular acts as a barrier or blender has been ongoing for decades (8, 9).

In this article, we describe direct measurements of lateral mixing in the Gulf Stream front, made by using the release and tracking of fluorescein dye. The observations were made as

part of the Scalable Lateral Mixing and Coherent Turbulence (LatMix) field campaign, which was devised to study the physics of currents at the submesoscale (0.1 to 10 km)—a range of motions between mesoscale eddies and small-scale, fully three-dimensional turbulence—and their effect on mixing (10, 11). At these scales, the circulation is characterized by fast-growing instabilities, strong nonlinearities, and vigorous overturning circulations in the surface boundary layer. These processes are thought to play an important role in setting the depth of the ocean mixed layer, dissipating the kinetic energy of the ocean circulation, facilitating the growth of phytoplankton, and sequestering carbon in the ocean (12–17). The submesoscale is well below the resolution of most prior work on lateral mixing in the Gulf Stream region—but it had been posited that submesoscale currents could also be crucial to the horizontal dispersal of tracers in the ocean, and one of the aims of the LatMix field campaign was to test this hypothesis. Here, we present evidence from a dye-release experiment in the Gulf Stream, which shows that near the surface, there can be significant exchange across the front, and we use high-resolution numerical

## Significance

**The Gulf Stream front separates the North Atlantic subtropical and subpolar ocean gyres, which have very distinct physical, biological, and chemical properties.** Exchange across the front is believed to be important for both ocean circulation and biological productivity; however, the physical mechanisms responsible are not fully understood. Here, we present direct observational evidence of enhanced mixing across the north wall of the Gulf Stream. High-resolution simulations suggest that the presence of the sharp density front, not typically resolved in ocean-circulation models, is central to generating the observed mixing. Interpreting the observations in terms of the flux of freshwater and nutrients across the Gulf Stream north wall suggests an important mechanism of exchange that has not been fully explored.

Author contributions: J.O.W., L.N.T., and J.R.T. designed the numerical simulations; J.R.T. performed numerical simulations; M.A.S. was responsible for the collection and analysis of the in situ dye observations; L.N.T., M.A.S., E.A.D., J.M.K., R.K.S., and C.M.L. designed and implemented the LatMix 2012 field campaign; J.O.W. led the analysis of results; J.O.W., L.N.T., M.A.S., J.R.T., E.A.D., J.M.K., R.K.S., and C.M.L. contributed to interpreting results; and J.O.W. wrote the paper with contributions from all authors.

The authors declare no competing interest.

This article is a PNAS Direct Submission.

Published under the [PNAS license](#).

Data deposition: Data related to this paper are available in Figshare (<https://doi.org/10.6084/m9.figshare.12567740>). Analysis code is publicly available at GitHub (<http://github.com/wenegrat/LATMIXDYE/releases/latest>).

<sup>1</sup>To whom correspondence may be addressed. Email: wenegrat@umd.edu.

This article contains supporting information online at <https://www.pnas.org/lookup/suppl/doi:10.1073/pnas.2005558117/-DCSupplemental>.

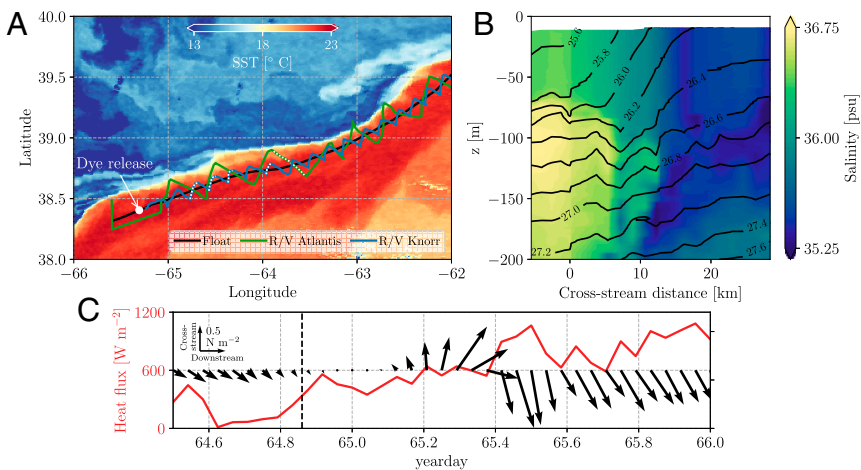


**Fig. 1.** Overview of the LatMix dye-release experiment along the Gulf Stream front. (A) Tracks of the Lagrangian float (black), *R/V Atlantis* (green), and *R/V Knorr* (blue) from yeardays 64 to 68, superimposed on sea-surface temperature from satellite observations on yearday 71 (color). The location of the dye release is indicated, and the *R/V Knorr* sections shown in Fig. 2 are indicated with dashed white lines. (B) Cross-frontal section of salinity (color) and density (black contours, with values indicated as  $\sigma = \rho - 1,000 \text{ kg} \cdot \text{m}^{-3}$ ), from the *R/V Atlantis* section indicated by the dashed white line in A. The horizontal coordinate is defined relative to the direction and position of the maximum depth-integrated observed velocity. (C) Net surface heat flux (red) and wind-stress vectors (black) calculated from shipboard observations. The stress vectors are shown in a coordinate system defined by the maximum depth-integrated currents, such that downstream is parallel and cross-stream is orthogonal, to the Gulf Stream jet (as shown in C, Inset). The nominal time of the dye release is indicated by the dashed black line.

simulations to understand the underlying submesoscale processes responsible for the observed dispersion. The essential mechanism we identify—shear dispersion generated by the interaction between submesoscale instabilities and time-varying boundary-layer turbulence—is likely ubiquitous across many regions of the world's oceans and adds another dimension to the long-standing question of whether the Gulf Stream acts as a barrier or a blender for intergyre exchange in the North Atlantic.

**Dye-Release Experiment.** The LatMix observational campaign was conducted along the north wall of the Gulf Stream front (Fig. 1) from 19 February to 17 March 2012 (yeardays 50 to 77). This work involved two global-class research vessels, the *R/V Atlantis* and the *R/V Knorr*, and an autonomously profiling Lagrangian (water-following) float (18). A neutrally buoyant mix of approximately 200 gallons of water and 100 kg of fluorescein dye was released at 25-m depth around the Lagrangian float. The

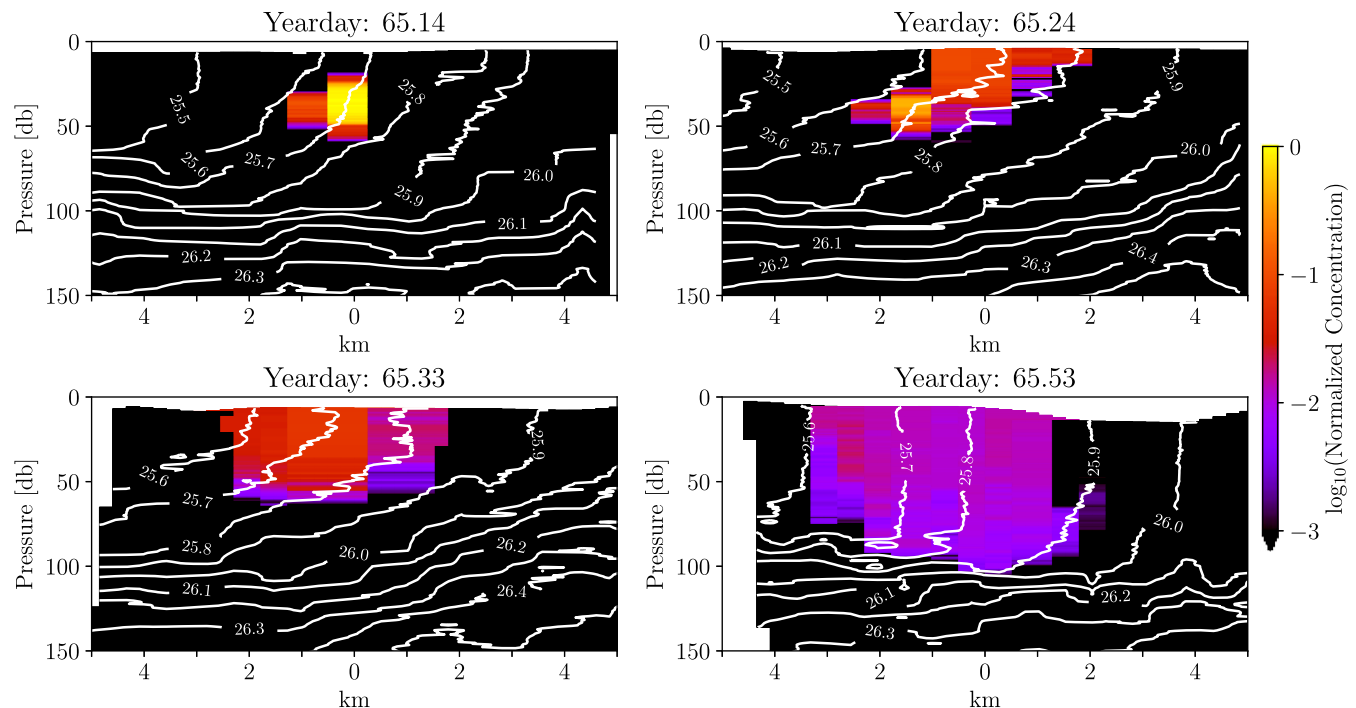


**Fig. 2.** Across Gulf Stream sections of observed dye concentration (color) and density (white contours, with values indicated as  $\sigma = \rho - 1,000 \text{ kg} \cdot \text{m}^{-3}$ ), showing the rapid horizontal dispersion of the dye across the front. In all sections, the cross-front direction is defined as orthogonal to the Lagrangian float's direction of travel, with distance relative to the position of the float. Concentrations are normalized to the maximum observed concentration across all surveys. An animation that includes additional sections is provided as [Movie S1](#).

evolution of the dye patch was then tracked by following the acoustically tracked position of the Lagrangian float. Measurements of dye concentration, water temperature, salinity, and velocity were taken from a ship-towed profiler in a series of cross-frontal surveys following the float location (Fig. 1) (19).

The dye was released on yearday 64.87 and immediately began spreading across the front (Fig. 2 and Movie S1). The dye center-of-mass remained on a density surface close to the initial injection density for the first 12 h following release, indicating that the initial cross-frontal spreading occurred predominantly

due to mixing along isopycnals, which were flattening out during the period of weak surface forcing (Fig. 1). On yearday 65.2, the surface winds intensified and rotated in the clockwise direction, exciting strong currents in the surface mixed layer, and enabling the explosive growth of symmetric instability across the ocean-surface boundary layer (11), a form of small-scale instability active at submesoscale ocean fronts (20). Symmetric instability is associated with an overturning circulation in the across-front direction, which can mix tracers along isopycnals (21) and enhance boundary-layer turbulence

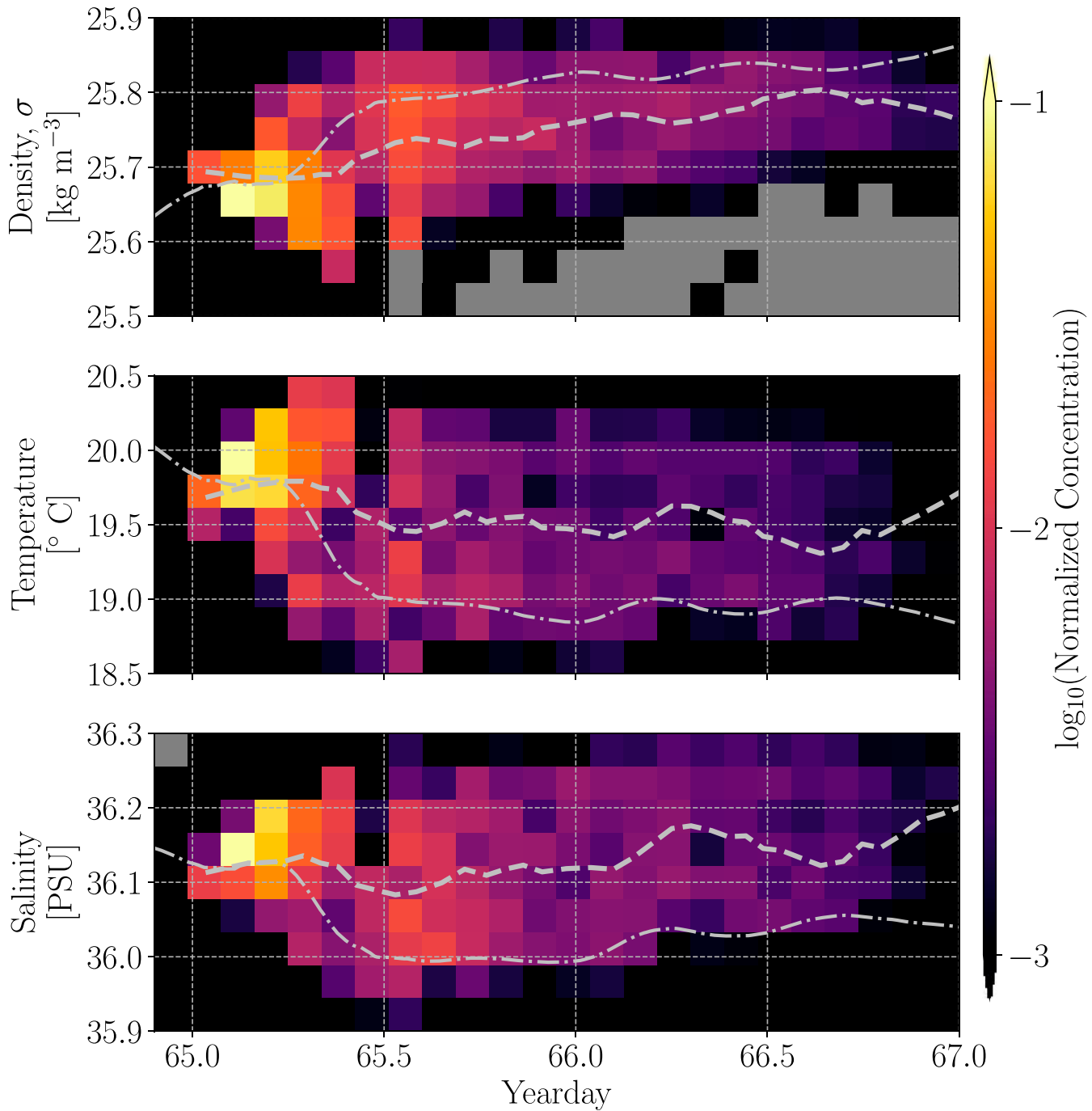


**Fig. 3.** Evolution of the dye from the *R/V Knorr* observations, showing the spread of the dye in density (Top), temperature (Middle), and salinity (Bottom) space as a function of time. The mean dye concentration of the binned observations is shown (color scale), normalized by the maximum observed concentration across all surveys. The values at the dye center-of-mass (dashed line) and from the Lagrangian float (dashed-dotted line) are also shown, both smoothed by using a cubic-spline over an approximately 8-h window. Gray areas indicate bins where data were not available.

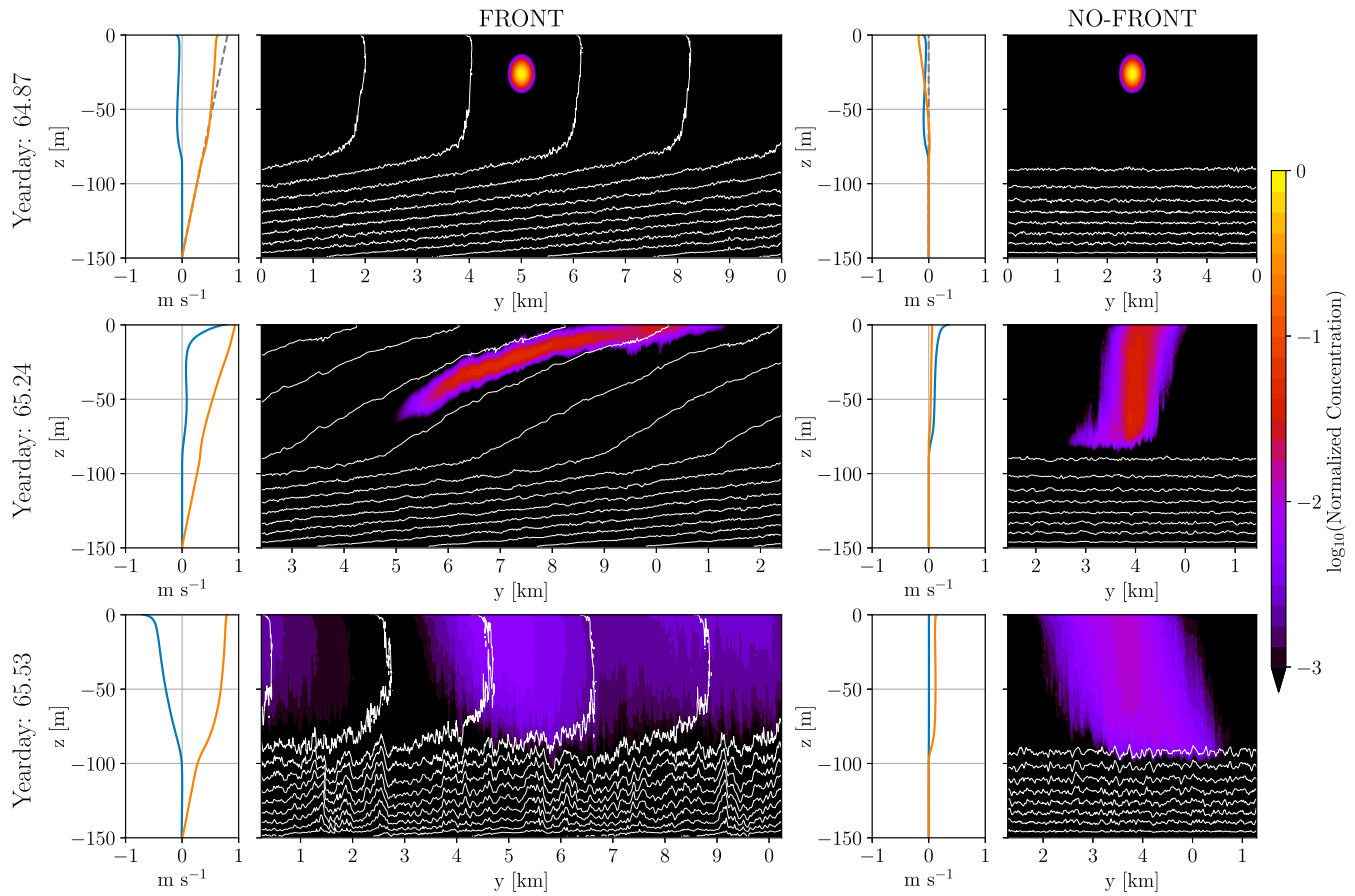


**Fig. 4.** Evolution of the passive numerical tracer in the LES run with a horizontal buoyancy gradient (FRONT; Left) and without a horizontal buoyancy gradient (NO-FRONT; Right). Snapshots of along-front averaged dye concentration (colorscale) and buoyancy (white contours, with interval equivalent to a change in density of  $0.1 \text{ kg} \cdot \text{m}^{-3}$ ) are shown at three times, as indicated to the left of each row. Profiles of the horizontally averaged across-front velocity (blue), along-front velocity (orange), and background geostrophic velocity (dashed gray) are also shown. Note that the  $y$  coordinate, which is periodic, shifts between plots such that the dye center of mass is centered. For computational efficiency (*SI Appendix*), the cross-front domain size varies between the FRONT and NO-FRONT run (10 and 5 km, respectively). An animation of the FRONT model run is provided as [Movie S2](#).

by generating secondary Kelvin–Helmholtz instabilities (13, 22). As the wind stress increased and the flow became more unstable to symmetric instability, the dye spread rapidly in the cross-frontal direction, and the center-of-mass moved toward colder and denser water (Figs. 2 and 3). The observations from the Lagrangian float evolved similarly; however, the changes in water-mass properties were more pronounced (Fig. 3). These differences are likely a consequence of the dye reflecting the integrated contributions of several pathways of mix-

ing (*SI Appendix*, Fig. S1), including vertical mixing across the boundary layer and horizontal mixing between the warm and salty Gulf Stream core and the cold and fresh subpolar gyre (Fig. 2).

The observed increase in horizontal variance of the dye concentration can be used to estimate the effective horizontal diffusivity of the flow (*SI Appendix*) (23). The rapid dispersion of the dye in the first 16 h after release suggests an average effective horizontal diffusivity in the across-front direction of

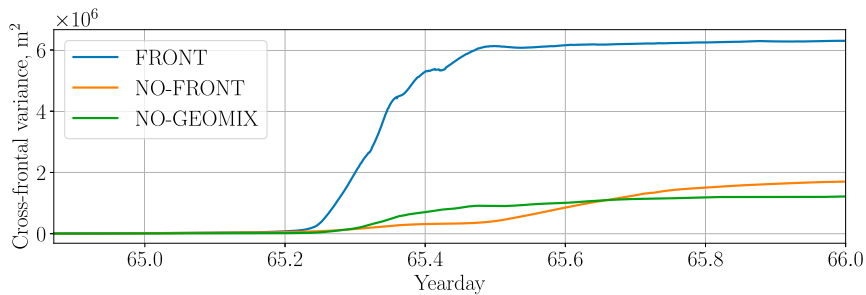


**Fig. 5.** Across-frontal dye variance,  $\overline{\sigma_y^2}$ , as a function of time for the three model simulations (calculated as described in *SI Appendix*). The effective horizontal diffusivity is proportional to the rate of increase of the variance; hence, the rapid increase of variance in the FRONT run due to shear dispersion indicates large horizontal diffusivities. The other runs develop little cross-frontal shear; hence, the dye variance increases slowly, and the effective diffusivities remain small.

$\kappa_h \approx 50 \text{ m}^2\text{s}^{-1}$  at horizontal length scales of 1 to 10 km. This estimate of  $\kappa_h$  is consistent in magnitude with estimates from surface drifter pair separation in this region (24) and estimates of the bulk diffusivity associated with lateral stirring by submesoscale streamers along the north wall of the Gulf Stream (9), but approximately an order of magnitude smaller than estimates of the diffusivity on scales of 10 to 100 km (8, 24, 25). These prior estimates have, however, tended to emphasize the role of advective stirring, a process which ultimately still requires an additional physical mechanism for generating across-isopycnal mixing in order to homogenize water properties. In contrast, the observations presented here provide direct evidence of irreversible tracer mixing across the Gulf Stream front itself. Further, the finding that these large magnitude horizontal diffusivities extend down to spatial scales of < 10 km suggests that these small scales may provide a large contribution to the total tracer flux, which is the product of the diffusivity and the horizontal tracer gradient, the latter of which scales inversely with the horizontal length scale.

**Numerical Simulations.** High-resolution large-eddy simulations (LESs) were used to isolate the physical processes responsible for the observed dye dispersion. The model was run in an idealized, horizontally periodic configuration with an imposed mean background horizontal density gradient that did not evolve in time (described in more detail in *SI Appendix*). Simulations were initialized on yearday 64.5 with a weakly stratified surface layer overlying a uniformly stratified interior, with parameters chosen to approximate the observations (11) and surface forcing provided by the surface heat fluxes and wind stress calculated from the shipboard observations (Fig. 1C). The most physically realistic “FRONT” run was configured with a mean background buoyancy gradient consistent with the observations ( $\partial b/\partial y = -5 \times 10^{-7} \text{ s}^{-2}$ , where the buoyancy is defined as  $b = -g\rho/\rho_o$  with  $g$  the gravitational acceleration,  $\rho$  the density, and  $\rho_o$  an average density). A “NO-FRONT” simulation was run without a mean horizontal buoyancy gradient ( $\partial b/\partial y = 0$ ) to test the contribution of the surface forcing alone. An additional run, designed as a numerical experiment to isolate the most important dynamical processes, was configured as in the FRONT run, but with model physics modified to not include the vertical advection of the along-front geostrophic flow (NO-GEOMIX; see *SI Appendix* for configuration details). In all simulations, a Gaussian patch of a passive numerical dye was released on yearday 64.87 at 25-m depth (Fig. 4), mimicking the dye deployment during the observational campaign (Fig. 2).

The FRONT run shows a dye evolution consistent with the observations (Fig. 4 and Movie S2). After release, the dye was rapidly mixed vertically throughout the weakly stratified upper 75 m. Vertically sheared cross-frontal flow then tilted over isopycnals and sheared the dye patch, converting horizontal dye gradients into vertical gradients, similar to the observed dye evolution (Fig. 2). Turbulence forced by strong surface winds, and secondary instabilities of symmetric instability, beginning around yearday 65.2 then homogenized the dye concentration in the vertical, causing an irreversible horizontal dispersion of the dye patch. The effective horizontal diffusivity reached peak values of  $\kappa_h \approx 380 \text{ m}^2\text{s}^{-1}$ , with an average value from release to the peak of the wind-forcing event (yeardays 64.87 to 65.5) of  $\kappa_h \approx 57 \text{ m}^2\text{s}^{-1}$ . This estimate agrees well with the observational estimate, but is slightly larger, potentially reflecting the more completely resolved dye dispersion in the numerical model, or missing model physics (for example, enhanced near-surface mixing due to surface waves which might act to reduce the near-surface cross-frontal shear).

In contrast to the FRONT run, in the NO-FRONT case, the dye patch was not tilted as strongly in the horizontal and, hence,

exhibited very little horizontal dispersion through the wind-mixing event (Fig. 5). The maximum estimated effective horizontal diffusivity was  $\kappa_h \approx 16 \text{ m}^2\text{s}^{-1}$ , and the average value was  $\kappa_h \approx 4 \text{ m}^2\text{s}^{-1}$ . These values are consistent in magnitude with scalings for isotropic turbulence generated by the surface wind-stress (26), i.e.,  $\kappa \sim u^* D$ , where  $u^* = \sqrt{|\tau|/\rho_o}$  is the friction velocity,  $\tau$  is the surface wind-stress vector, and  $D$  is the boundary

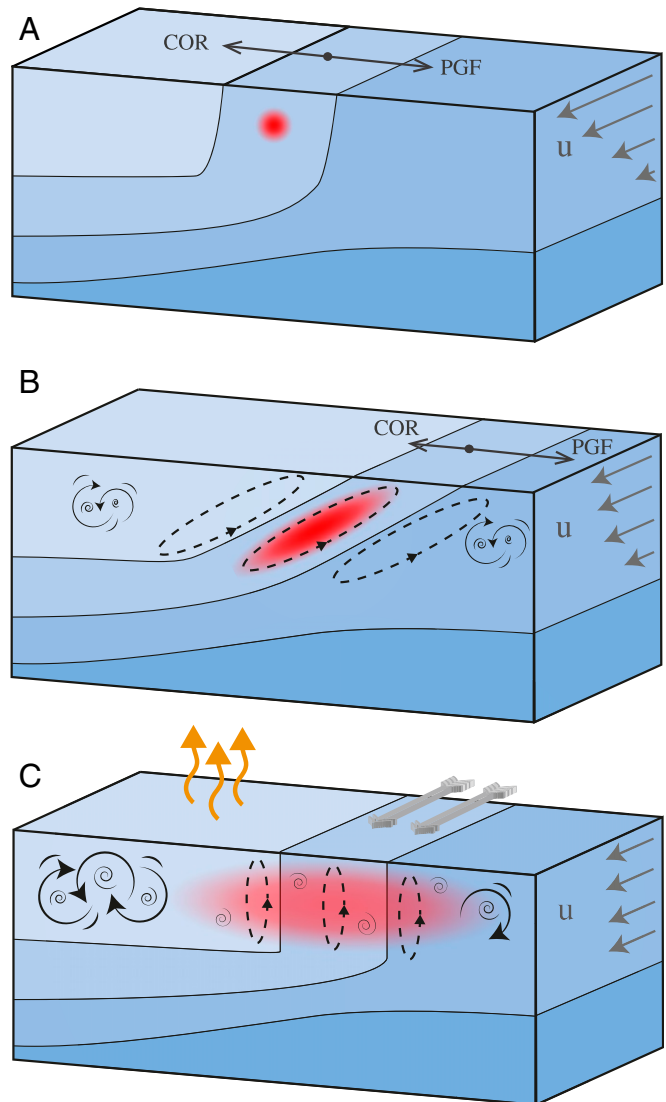


**Fig. 6.** Schematic of the shear-dispersion mechanism active at a submesoscale front. (A) Initially, the flow is in geostrophic balance, with Coriolis (COR) and across-front pressure gradient forces (PGF) canceling one another. A patch of passive tracer is shown in red. (B) Turbulence, and symmetric instability overturning cells (dashed lines), in the surface boundary layer mix away the thermal wind shear, disrupting the geostrophic balance by reducing the Coriolis force and allowing flow down the pressure gradient. Cross-frontal flow tilts over isopycnals and shears out the tracer patch. (C) Surface heat fluxes (orange arrows) or destabilizing winds (gray arrows) generate near-surface turbulence. When this becomes sufficiently strong to overcome the restratifying tendency of the cross-frontal advection of density, the tracer is mixed vertically across isopycnals. In each image, the profile of along-front velocity in the center of the front is shown projected on the right plane.

layer depth, which implies an average diffusivity of order  $1 \text{ m}^2 \text{s}^{-1}$  (using  $u^* \sim 0.01 \text{ m s}^{-1}$  and  $D \sim 100 \text{ m}$ , typical of these observations). These diffusivities are much smaller than those of the observations and FRONT run, indicating that the surface forcing alone was insufficient to generate the observed dispersion and that the presence of the buoyancy front was enhancing horizontal dispersion by at least an order of magnitude.

The sequence of dye evolution in the FRONT run was consistent with the classic Taylor shear-dispersion mechanism (27), whereby advection of a tracer by a sheared velocity field, plus turbulent mixing in the direction of the velocity gradient, generates an effective turbulent dispersion in the direction of the flow (Fig. 6). Here, the generation mechanism for the cross-frontal shear was vertical mixing of the geostrophically balanced along-front flow, which through the thermal wind balance had a uniform vertical shear of magnitude  $\partial u_g / \partial z = -f^{-1} \partial \bar{b} / \partial y = 5.4 \times 10^{-3} \text{ s}^{-1}$ , where  $f$  is the Coriolis frequency. Vertical mixing of momentum, generated by both the atmospheric forcing and by the symmetric instability overturning cells, acted to homogenize the velocity profile in the surface mixed layer (Fig. 4). This disrupted the geostrophic balance, generating a vertically sheared inertial oscillation that rotated into the cross-frontal plane (*SI Appendix*), shearing the dye patch and allowing subsequent turbulence to irreversibly mix the dye across buoyancy surfaces (Figs. 4 and 6). Theory suggests that the strength of the effective diffusivity generated by shear dispersion of an oscillatory shear flow (with magnitude proportional to the geostrophic shear) (28) or by subinertial flow at a mixed-layer

front (29–31) should in both cases scale with the square of the horizontal buoyancy gradient,  $\kappa_h \propto |\nabla_h b|^2$ , highlighting the enhancement of this mechanism at submesoscale fronts where the buoyancy gradients are large.

In simulation NO-GEOMIX, this disruption of the geostrophic balance was artificially suppressed by removing the vertical advection of geostrophic momentum, which stops mixing due to resolved turbulence. As a result, the cross-frontal flow in NO-GEOMIX developed little vertical shear, and, hence, the dye evolved similarly to the NO-FRONT run with minimal tilting of the dye patch through day 65.2 (Fig. 7). The subsequent wind forcing, in turn, generated limited across-isopycnal mixing of the dye, leading to effective diffusivities in NO-GEOMIX that were similar to the NO-FRONT case (Fig. 5). The mixing of geostrophic momentum is therefore central to generating the across-frontal shear flow and the concomitant shear dispersion, evident in the observations and FRONT run. More generally, however, the essential mechanism we have outlined—shear dispersion due to a combination of cross-frontal shear flow and vertical mixing—can arise through a variety of dynamical mechanisms at sharp fronts and is therefore likely a generic feature of regions with active submesoscales. We comment more on this below.

## Discussion

The observations presented here provide unique direct wintertime observations of cross-frontal dispersion across the Gulf Stream front, the boundary between the North Atlantic

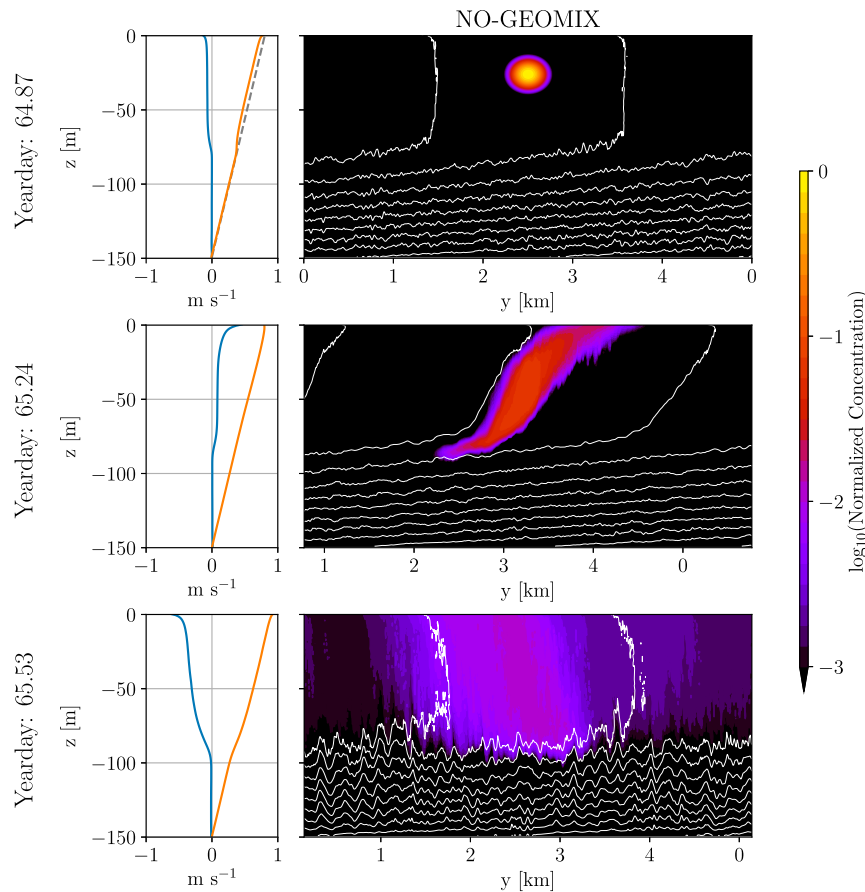


**Fig. 7.** Evolution of the passive tracer in the NO-GEOMIX simulation. Snapshots are shown at three times (indicated to the left of each row) for dye concentration (colorscale) and buoyancy (white contours). Profiles of the horizontally averaged velocity are also shown (blue, across-front velocity; orange, along-front velocity; and dashed gray in top row, background geostrophic velocity). Note that the horizontal spatial coordinate ( $y$ ), which is periodic, shifts between plots to center the dye patch.

subtropical and subpolar gyres. These water masses have distinct physical and biogeochemical properties (Fig. 1 and *SI Appendix*, Fig. S4); hence, the observed dye dispersion suggests that submesoscale fronts are acting to enhance fluxes of freshwater and nutrients between the subpolar gyre and the Gulf Stream core. In the North Atlantic, these cross-frontal fluxes have the potential to significantly affect the formation of subtropical-mode water, which provides a pathway for the export of heat and carbon from the surface ocean to the interior, and to affect carbon sequestration through the ocean biological pump (3–6).

As an example, it is informative to evaluate the potential contribution of shear dispersion at submesoscale fronts to the salinity budget of the subtropical mode water formed in the Gulf Stream, which is not currently well understood, despite the implications for decadal climate variability (6). The horizontal diffusive flux of salinity in the mixed layer will scale as  $\kappa_h D \Delta S / L$ , where  $\Delta S$  is the change in salinity across the front, and  $L$  is the cross-stream length scale. The last three of these terms can be estimated directly from the observations as  $D = 100$  m,  $\Delta S = -1$  practical salinity unit (psu), and  $L = 10$  km (Fig. 1). A reasonable first estimate for the diffusivity is  $\kappa_h = 50 \text{ m}^2 \text{s}^{-1}$ , based on the observations, although we emphasize that a variety of factors will affect the average diffusivity generated by shear dispersion (as discussed in more detail in *SI Appendix*). Using these estimates, and integrating over a 1,200-km segment of the Gulf Stream (for comparison with ref. 6), indicates that shear dispersion at submesoscale fronts could provide a salinity flux of approximately  $-6 \times 10^5 \text{ psu} \cdot \text{m}^3 \text{s}^{-1}$  across the Gulf Stream front. This is a significant portion of the  $-1.4 \times 10^6 \text{ psu} \cdot \text{m}^3 \text{s}^{-1}$  estimated from observations as necessary to close the salinity budget of the north Atlantic subtropical mode water (6), particularly given the large observational uncertainty.

Similar estimates can also be formed for the flux of nutrients such as phosphate and nitrate, which indicates that submesoscale shear dispersion may likewise provide a contribution to exchange across the north wall front that is comparable to prior estimates of lateral advective nutrient fluxes (*SI Appendix*). Current uncertainties in the spatial, and temporal, distribution of these frontal processes make it difficult to infer the ultimate fate of these tracers, which will have trajectories determined by a combination of lateral mixing processes and advection by the fast-flowing

Gulf Stream jet. However, the observed rapid dispersion, and irreversible mixing across isopycnals, suggest that submesoscale shear dispersion should be considered alongside the more well-studied advective mechanisms, such as mesoscale eddy stirring and wind-driven transport (3, 4, 8), for intergyre mixing at the Gulf Stream front.

The physical mechanism identified here as responsible for the observed rapid tracer dispersion, shear dispersion generated by the mixing of geostrophic momentum, will be enhanced at sharp submesoscale fronts where strong buoyancy gradients imply large thermal wind shears. These fronts are also often susceptible to a variety of fast-growing instabilities that contribute to the mixing of geostrophic momentum and the generation of turbulence (20, 22, 32), further enhancing the cross-frontal shear dispersion. However, beyond the particular dynamical progression outlined here, the basic mechanism of shear dispersion due to a combination of sheared cross-frontal flows and time-varying turbulent mixing of the boundary layer is likely a generic feature of submesoscale fronts and is robust to both the details of the turbulent mixing and the origin of the shear flow (28, 29, 33). For example, strong cross-frontal shear flows can be generated at sharp fronts through symmetric instability (as documented here), baroclinic mixed-layer instabilities (34), turbulent mixing (35), or simply lateral slumping due to gravity (36). The observed rapid dye dispersion presented here therefore also provides direct observational confirmation of the hypothesized role of shear dispersion at the submesoscale in reducing tracer gradients in the turbulent surface mixed layer (e.g., compare the salinity gradient above and below 75-m depth in Fig. 1B; and see ref. 37). Along the Gulf Stream, this mechanism has the potential to play an important role in driving exchange across the north wall front, motivating the need for the development of a more complete understanding of submesoscale-turbulence interactions and the cumulative effects of shear dispersion at sharp ocean fronts.

**ACKNOWLEDGMENTS.** We thank the crews of the *R/V Knorr* and *R/V Atlantis* for making these observations possible. This work was supported by the Scalable Lateral Mixing and Coherent Turbulence Departmental Research Initiative and the Physical Oceanography Program of the Office of Naval Research, program officers Terri Paluszakiewicz and Scott Harper. Comments and suggestions from Baylor Fox-Kemper and an anonymous reviewer improved this manuscript.

1. R. G. Williams, M. J. Follows, The Ekman transfer of nutrients and maintenance of new production over the North Atlantic. *Deep Sea Res. Oceanogr. Res. Pap.* **45**, 461–489 (1998).
2. A. Oschlies, Nutrient supply to the surface waters of the North Atlantic: A model study. *J. Geophys. Res.* **107**, 3046 (2002).
3. J. B. Palter, M. S. Lozier, J. L. Sarmiento, R. G. Williams, The supply of excess phosphate across the Gulf Stream and the maintenance of subtropical nitrogen fixation. *Global Biogeochem. Cycles* **25**, GB4007 (2011).
4. R. T. Letscher, F. Primeau, J. K. Moore, Nutrient budgets in the subtropical ocean gyres dominated by lateral transport. *Nat. Geosci.* **9**, 815–819 (2016).
5. A. Yamamoto et al., Roles of the ocean mesoscale in the horizontal supply of mass, heat, carbon, and nutrients to the Northern Hemisphere subtropical gyres. *J. Geophys. Res.: Oceans* **123**, 7016–7036 (2018).
6. T. M. Joyce, L. N. Thomas, W. K. Dewar, J. B. Girton, Eighteen degree water formation within the Gulf stream during CLIMODE. *Deep Sea Res. Part II Top. Stud. Oceanogr.* **91**, 1–10 (2013).
7. G. Haller, D. Karrasch, F. Kogelbauer, Material barriers to diffusive and stochastic transport. *Proc. Natl. Acad. Sci. U.S.A.* **115**, 9074–9079 (2018).
8. A. S. Bower, H. T. Rossby, J. L. Lillibridge, The Gulf Stream—Barrier or blender? *J. Phys. Oceanogr.* **15**, 24–32 (1985).
9. J. M. Klymak et al., Submesoscale streamers exchange water on the north wall of the Gulf Stream. *Geophys. Res. Lett.* **43**, 1226–1233 (2016).
10. A. Y. Shcherbina et al., The LatMix summer campaign: Submesoscale stirring in the upper ocean. *Bull. Am. Meteorol. Soc.* **96**, 1257–1279 (2015).
11. L. N. Thomas et al., Symmetric instability, inertial oscillations, and turbulence at the Gulf Stream front. *J. Phys. Oceanogr.* **46**, 197–217 (2016).
12. L. N. Thomas, A. Tandon, A. Mahadevan, “Submesoscale processes and dynamics” in *Geophysical Monograph Series*, M. W. Hecht, H. Hasumi, Eds. (American Geophysical Union, Washington, DC, 2008), vol. 177, pp. 17–38.
13. E. D’Asaro, C. Lee, L. Rainville, R. Harcourt, L. Thomas, Enhanced turbulence and energy dissipation at ocean fronts. *Science* **332**, 318–322 (2011).
14. M. Lévy, R. Ferrari, P. J. S. Franks, A. P. Martin, P. Rivière, Bringing physics to life at the submesoscale. *Geophys. Res. Lett.* **39**, L14602 (2012).
15. M. M. Omand et al., Eddy-driven subduction exports particulate organic carbon from the spring bloom. *Science* **348**, 222–225 (2015).
16. A. Mahadevan, The impact of submesoscale physics on primary productivity of plankton. *Annu. Rev. Mar. Sci.* **8**, 161–184 (2016).
17. J. C. McWilliams, Submesoscale currents in the ocean. *Proc. R. Soc. A: Math., Phys. Eng. Sci.* **472**, 20160117 (2016).
18. E. A. D’Asaro, Performance of autonomous Lagrangian floats. *J. Atmos. Ocean. Technol.* **20**, 896–911 (2003).
19. J. Wenegrat et al., Data for “Enhanced mixing across the gyre boundary at the Gulf Stream front.” Figshare. <https://doi.org/10.6084/m9.figshare.12567740>. Deposited 25 June 2020.
20. J. R. Taylor, R. Ferrari, Buoyancy and wind-driven convection at mixed layer density fronts. *J. Phys. Oceanogr.* **40**, 1222–1242 (2010).
21. S. Bachman, B. Fox-Kemper, J. Taylor, L. Thomas, Parameterization of frontal symmetric instabilities. I: Theory for resolved fronts. *Ocean Model.* **109**, 72–95 (2017).
22. J. R. Taylor, R. Ferrari, On the equilibration of a symmetrically unstable front via a secondary shear instability. *J. Fluid Mech.* **622**, 103–113 (2009).
23. M. A. Sundermeyer, J. R. Ledwell, Lateral dispersion over the continental shelf: Analysis of dye release experiments. *J. Geophys. Res.: Oceans* **106**, 9603–9621 (2001).
24. R. Lumpkin, S. Eliopon, Surface drifter pair spreading in the North Atlantic. *J. Geophys. Res.* **115**, C12017 (2010).
25. I. I. Rypina, I. Kamenkovich, P. Berloff, L. J. Pratt, Eddy-induced particle dispersion in the near-surface North Atlantic. *J. Phys. Oceanogr.* **42**, 2206–2228 (2012).
26. W. G. Large, J. C. McWilliams, S. C. Doney, Oceanic vertical mixing: A review and a model with a nonlocal boundary layer parameterization. *Rev. Geophys.* **32**, 363 (1994).

27. G. I. Taylor, Dispersion of soluble matter in solvent flowing slowly through a tube. *Proc. R. Soc. Lond. Math. Phys. Sci.* **219**, 186–203 (1953).
28. W. R. Young, P. B. Rhines, C. J. R. Garrett, Shear-flow dispersion, internal waves and horizontal mixing in the ocean. *J. Phys. Oceanogr.* **12**, 515–527 (1982).
29. W. R. Young, The subinertial mixed layer approximation. *J. Phys. Oceanogr.* **24**, 1812–1826 (1994).
30. L. Chen, W. R. Young, Density compensated thermohaline gradients and diapycnal fluxes in the mixed layer. *J. Phys. Oceanogr.* **25**, 3064–3075 (1995).
31. M. N. Crowe, J. R. Taylor, The evolution of a front in turbulent thermal wind balance. Part 1. Theory. *J. Fluid Mech.* **850**, 179–211 (2018).
32. A. F. Thompson et al., Open-ocean submesoscale motions: A full seasonal cycle of mixed layer instabilities from gliders. *J. Phys. Oceanogr.* **46**, 1285–1307 (2016).
33. R. Ferrari, W. R. Young, On the development of thermohaline correlations as a result of nonlinear diffusive parameterizations. *J. Mar. Res.* **55**, 1069–1101 (1997).
34. B. Fox-Kemper, R. Ferrari, R. Hallberg, Parameterization of mixed layer eddies. Part I: Theory and diagnosis. *J. Phys. Oceanogr.* **38**, 1145–1165 (2008).
35. J. O. Wenegrat, M. J. McPhaden, Wind, waves, and fronts: Frictional effects in a generalized Ekman model. *J. Phys. Oceanogr.* **46**, 371–394 (2016).
36. A. Tandon, C. Garrett, Mixed layer restratification due to a horizontal density gradient. *J. Phys. Oceanogr.* **24**, 1419–1424 (1994).
37. D. L. Rudnick, R. Ferrari, Compensation of horizontal temperature and salinity gradients in the ocean mixed layer. *Science* **283**, 526–529 (1999).